

# NbReSi: A Noncentrosymmetric Superconductor with Large Upper Critical Field

H. Su,<sup>1,2</sup> T. Shang,<sup>3,\*</sup> F. Du,<sup>1,2</sup> C. F. Chen,<sup>1,2</sup> H. Q. Ye,<sup>1,2</sup>  
X. Lu,<sup>1,2,4</sup> C. Cao,<sup>1,5</sup> M. Smidman,<sup>1,2</sup> and H. Q. Yuan<sup>1,2,4,6,†</sup>

<sup>1</sup>Center for Correlated Matter and Department of Physics, Zhejiang University, Hangzhou 310058, China

<sup>2</sup>Zhejiang Province Key Laboratory of Quantum Technology and Device,  
Department of Physics, Zhejiang University, Hangzhou 310058, China

<sup>3</sup>Key Laboratory of Polar Materials and Devices (MOE),

School of Physics and Electronic Science, East China Normal University, Shanghai 200241, China

<sup>4</sup>Collaborative Innovation Center of Advanced Microstructures, Nanjing University, Nanjing, 210093, China

<sup>5</sup>Condensed Matter Group, Department of Physics,  
Hangzhou Normal University, Hangzhou 311121, China

<sup>6</sup>State Key Laboratory of Silicon Materials, Zhejiang University, Hangzhou 310058, China

(Dated: November 12, 2021)

We report the discovery of superconductivity in noncentrosymmetric NbReSi, which crystallizes in a hexagonal ZrNiAl-type crystal structure with space group  $P6_3/m$  (No. 189). Bulk superconductivity, with  $T_c = 6.5$  K was characterized via electrical-resistivity, magnetization, and heat-capacity measurements. The low-temperature electronic specific heat suggests a fully gapped superconducting state in NbReSi, while a large upper critical field of  $\mu_0 H_{c2}(0) \sim 12.6$  T is obtained, which is comparable to the weak-coupling Pauli limit. The electronic band-structure calculations show that the density of states at the Fermi level are dominated by Re and Nb  $d$ -orbitals, with a sizeable band splitting induced by the antisymmetric spin-orbit coupling. NbReSi represents another candidate material for revealing the puzzle of time-reversal symmetry breaking observed in some Re-based superconductors and its relation to the lack of inversion symmetry.

## INTRODUCTION

Noncentrosymmetric superconductors (NCSC), where the crystal structure lacks an inversion center, have been widely investigated after the discovery of superconductivity (SC) in heavy fermion compound CePt<sub>3</sub>Si [1]. The lack of inversion symmetry gives rise to antisymmetric spin orbit coupling (ASOC), which causes band splitting near the Fermi level. As a consequence, the superconducting pairing may be a mixture of spin singlet and spin triplet states [2, 3]. Unconventional physical properties closely related to such a mixed pairings have been observed in NCSCs, e.g., superconducting gap nodes [4–8], multiband SC [9–12]. On the other hand, large upper critical field exceeding the Pauli limit is observed in some NCSCs [1, 13–16].

Unconventional SC has been reported in different families of heavy fermion NCSCs, e.g., CePt<sub>3</sub>Si [1], CeTX<sub>3</sub> ( $T$  = transition metal,  $X$  = Si or Ge) [17–20] and UIr [21]. In these compounds, the strong correlations or magnetic fluctuations can hinder the identification of the role played by the broken inversion symmetry in giving rise to unconventional superconducting properties, and as such non-magnetic weakly-correlated NCSCs have been investigated. For instance, while Li<sub>2</sub>Pd<sub>3</sub>B behaves as a fully-gapped two-band superconductor, an increase of ASOC (via Pt-for-Pd substitution) leads to Li<sub>2</sub>Pt<sub>3</sub>B being a nodal superconductor, indicating a dominant triplet component [4, 22, 23]. In addition, a growing number of NCSCs have also been found to exhibit time-reversal symmetry (TRS) breaking (i.e., spontaneous magnetic fields) in their superconducting state, such as, CaPtAs [7],

LaNiC<sub>2</sub> [24], Zr<sub>3</sub>Ir [25], and La<sub>7</sub>TM<sub>3</sub> ( $TM$  = Ni, Rh, Pd, Ir) [26–29]. In some of these NCSCs, the ASOC is rather weak, and there is evidence for fully gapped superconductivity (SC) similar to  $s$ -wave superconductors, and the origin of the TRS breaking is generally not yet well understood.

Recently, the  $\alpha$ -Mn-type noncentrosymmetric Re-based superconductors have attracted considerable interest, mainly due to the observation of broken time reversal symmetry at the onset of SC [30–33]. On the other hand, in a few Re-free  $\alpha$ -Mn-type superconductors, e.g., Mg<sub>10</sub>Ir<sub>19</sub>B<sub>16</sub> and Nb<sub>0.5</sub>Os<sub>0.5</sub> [34, 35], TRS is preserved. Recent muon-spin relaxation ( $\mu$ SR) studies on Re<sub>1-x</sub>Mo<sub>x</sub> alloys revealed that spontaneous magnetic fields below  $T_c$  were observed only in elementary rhenium and in Re<sub>0.88</sub>Mo<sub>0.12</sub> [33, 36], which both have centrosymmetric crystal structures. By contrast, TRS is preserved in the Re<sub>1-x</sub>Mo<sub>x</sub> alloys for  $x > 0.12$ , independent of their centro- or noncentrosymmetric crystal structures [36]. Moreover, TRS is preserved in both centro- or noncentrosymmetric rhenium-boron superconductors [37]. All these results suggest that a noncentrosymmetric structure and thus the ASOC is not essential in realizing TRS breaking in Re-based superconductors, and its origins require further investigations.

The ZrNiAl-type compounds are another important family of noncentrosymmetric superconductors. (Zr,Hf)RuP [38] and ZrRu(As,Si) [39, 40], which were synthesized under high pressure, exhibit relatively high superconducting transition temperatures  $T_c \sim 10$  K. Both ZrRuAs [41] and LaPdIn [42] are fully-gapped superconductors with preserved TRS. NbReSi also crys-

tallizes in a ZrNiAl-type structure [43], but its physical properties are not yet well studied.

In this paper, we report a systematic study of the superconducting properties of noncentrosymmetric NbReSi by means of electrical-resistivity, magnetization, and heat-capacity measurements, as well as by electronic band-structure calculations. It is found that NbReSi is a fully-gapped superconductor with a superconducting transition temperature  $T_c = 6.5$  K and exhibits a large upper critical field of  $\mu_0 H_{c2} = 12.6$  T. The electronic band-structure calculations suggest a sizable band splitting caused by the ASOC.

## EXPERIMENTAL DETAILS

Polycrystalline NbReSi samples were prepared by arc melting stoichiometric amounts of Nb slugs (99.95%, Alfa Aesar), Re powders (99.99%, Alfa Aesar) and Si chunks (99.9999%, Alfa Aesar) in high-purity argon atmosphere, with Ti metal used as oxygen getter. The samples were flipped and remelted several times to improve the homogeneity. The crystal structure and phase purity were checked by powder x-ray diffraction (XRD) measured on a Rigaku diffractometer with Cu  $K\alpha$  radiation. The electrical-resistivity and heat-capacity measurements were performed on Quantum Design Physical Property Measurement System (PPMS) with a  $^3\text{He}$  cryostat. The magnetization measurements were carried out using Quantum Design Magnetic Property Measurement System (MPMS). The electronic band-structures were calculated by means of the density-functional theory (DFT) implemented in the Vienna **ab-initio** simulation package (VASP). The Perdew-Burke-Ernzerhoff (PBE) functional in the generalized gradient approximation was employed.

## RESULTS AND DISCUSSION

Powder XRD patterns of NbReSi measured at room temperature are shown in Fig. 1(a). Almost all the reflections can be well indexed by a hexagonal ZrNiAl-type structure with space group  $P\bar{6}2m$  (No. 189) (see vertical green bars). The peaks with rather weak intensity [marked by star symbols in Fig. 1(a)] corresponds to additional phases, which could be due to binary Re-Si or Nb-Si phases that do not lead to extrinsic transitions. The determined lattice parameters  $a = 6.7194(3)$  Å and  $c = 3.4850(2)$  Å are consistent with the previous reports [43]. The crystal structure of NbReSi is shown in Fig. 1(b), where the NbSi- and ReSi-layers are alternately stacked along the  $c$ -axis. In the unit cell, Nb and Re atoms occupy noncentrosymmetric  $3g$  and  $3f$  sites, while the two Si-sites ( $2d$  and  $1a$ ) are centrosymmetric.

The temperature dependence of the electrical resistivity  $\rho(T)$  [see inset of Fig. 2(a)], collected in zero mag-

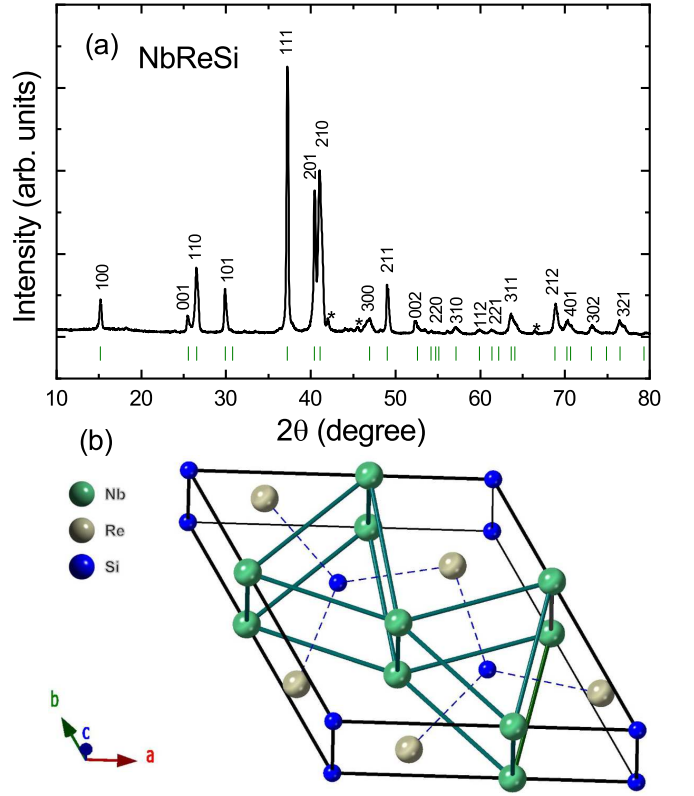


FIG. 1. (a) Powder x-ray diffraction pattern of NbReSi. The vertical bars are the calculated Bragg reflection positions for a ZrNiAl-type crystal structure. (b) Crystal structure of NbReSi. Nb, Re, and Si atoms are shown by green, grey, and blue spheres, respectively.

netic field from 2 to 300 K, reveals a metallic character of NbReSi. The main panel of Fig. 2(a) shows the enlarged plot of  $\rho(T)$  below 10 K. There is a sharp superconducting transition below  $T_c^{\text{onset}} = 6.9$  K, reaching zero resistivity at  $T_c^{\text{zero}} = 6.5$  K, which is slightly higher than the previous reported  $T_c$  value (i.e., 5.1 K) [46]. The bulk SC of NbReSi was confirmed by the magnetic susceptibility measurements. The temperature dependence of the  $dc$  magnetic susceptibility  $\chi(T)$  of NbReSi, measured in a field of 1 mT under field-cooled (FC) and zero-field-cooled (ZFC) processes, is shown in Fig. 2(b). A clear diamagnetic signal appears below the superconducting transition at  $T_c = 6.5$  K. The large differences between the FC- and ZFC-susceptibilities are typical of type-II superconductors, where the magnetic flux is pinned once the material is cooled in an applied field. After accounting for the demagnetization factor, the superconducting shielding fraction is close to 100%.

To determine the lower critical field  $H_{c1}$ , the field-dependent magnetization  $M(H)$  of NbReSi was collected at various temperatures up to  $T_c$  using a ZFC-protocol. Some representative  $M(H)$  curves are shown in the inset of Fig. 3. For each temperature,  $H_{c1}$  was determined as the value where  $M(H)$  deviates from linearity (solid line

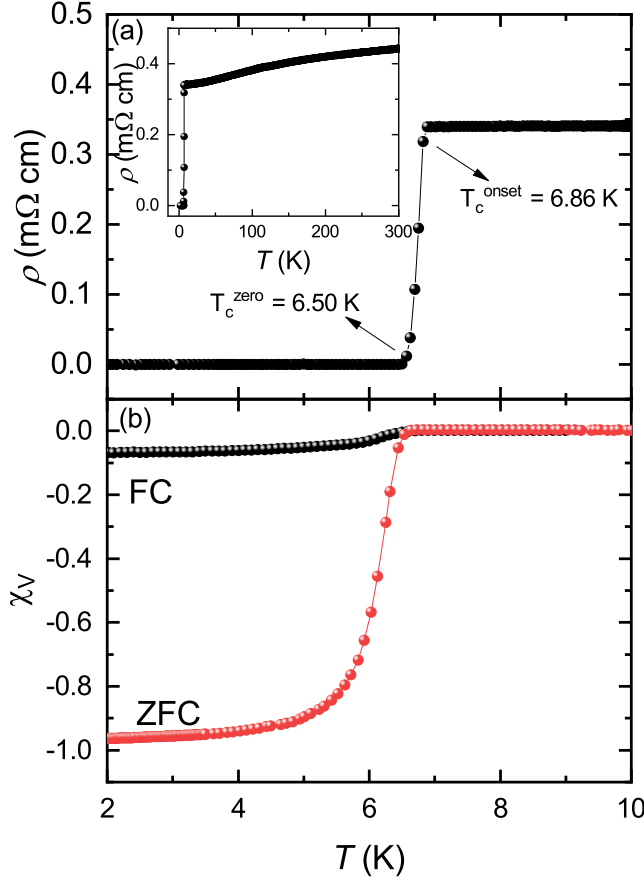


FIG. 2. (a) Temperature dependence of the electrical resistivity of NbReSi below 10 K. The data between 2 and 300 K is shown in the inset. (b) Temperature dependence of the magnetic susceptibility, measured in an applied field of 1 mT using both the ZFC and FC protocols. The demagnetization factor is estimated to be about 0.2, considering the cuboid sample has the shape of  $c/a \sim 1.4$  and  $c/b \sim 2.7$  with field applied along  $c$ -direction [44, 45].

in the inset of Fig. 3). Taking into account the demagnetization factor, the  $H_{c1}$  are summarized in the main panel of Fig. 3 as a function of temperature, where the zero-temperature lower critical field  $\mu_0 H_{c1}(0) = 10.1(1)$  mT is also determined.

To study the SC of NbReSi, we also performed heat-capacity measurements. The jump in the specific heat at  $T_c$  again demonstrates bulk SC in NbReSi (see Fig. 4). In the normal state, the specific heat can be analyzed using  $C(T)/T = \gamma_n + \beta T^2$ , where  $\gamma_n$  is the normal-state electronic specific-heat coefficient and  $\beta T^2$  represents the phonon contribution. As shown by the solid line in the inset of Fig. 4,  $\gamma_n = 8.23(2)$  mJ mol<sup>-1</sup> K<sup>-2</sup> and  $\beta = 0.160(3)$  mJ mol<sup>-1</sup> K<sup>-4</sup> were obtained for NbReSi. The Debye temperature  $\Theta_D = 331$  K was calculated via  $\Theta_D = (12\pi^4 Rn/5\beta)^{1/3}$ , where  $R = 8.314$  J mol<sup>-1</sup> K<sup>-1</sup> is the gas constant and  $n = 3$  is the number of atoms per formula. The electron-phonon coupling constant  $\lambda_{ep}$  was

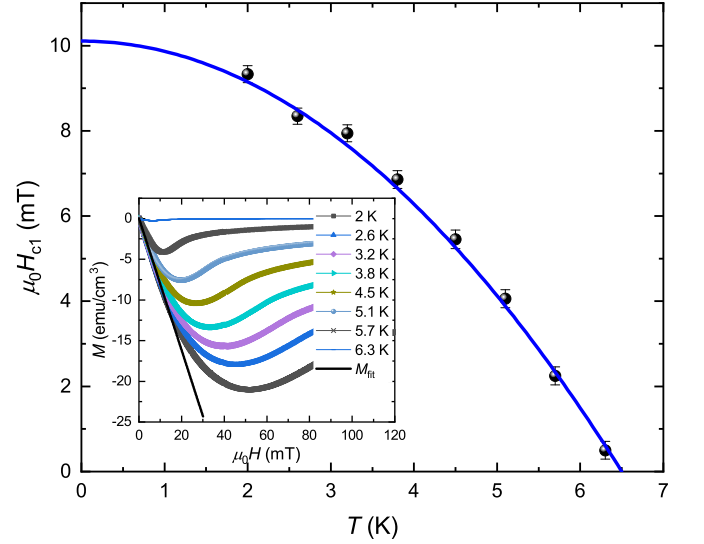


FIG. 3. Lower critical fields  $H_{c1}$  vs. temperature of NbReSi. Solid line is a fit to  $\mu_0 H_{c1}(T) = \mu_0 H_{c1}(0)[1 - (T/T_c)^2]$ . The inset plots the field-dependent magnetization recorded at various temperatures. For each temperature,  $H_{c1}$  was determined as the value where  $M(H)$  starts deviating from linearity (see black solid line).

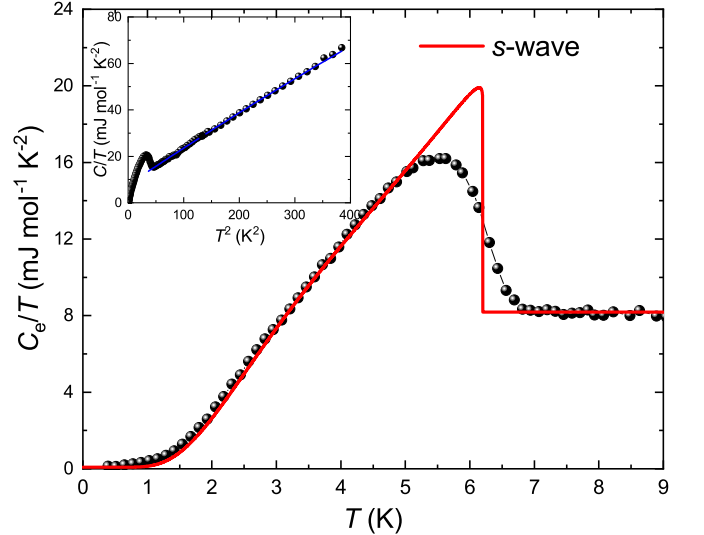


FIG. 4. Zero-field electronic specific heat  $C_e/T$  versus temperature for NbReSi. The red solid line through the data represents a fit to an  $s$ -wave model with a single gap. The inset shows the total specific heat  $C/T$  versus  $T^2$ , where the blue line is a fit to  $C/T = \gamma_n + \beta T^2$ .

estimated to be 0.66 using the McMillan formula [47]:

$$\lambda_{ep} = \frac{1.04 + \mu^* \ln(\Theta_D/1.45T_c)}{(1 - 0.62\mu^*) \ln(\Theta_D/1.45T_c) - 1.04}, \quad (1)$$

where the Coulomb pseudo-potential  $\mu^*$  is fixed to a typical value of 0.13 for metallic materials. The density of states (DOS) at the Fermi level  $N(E_F)$  can be esti-

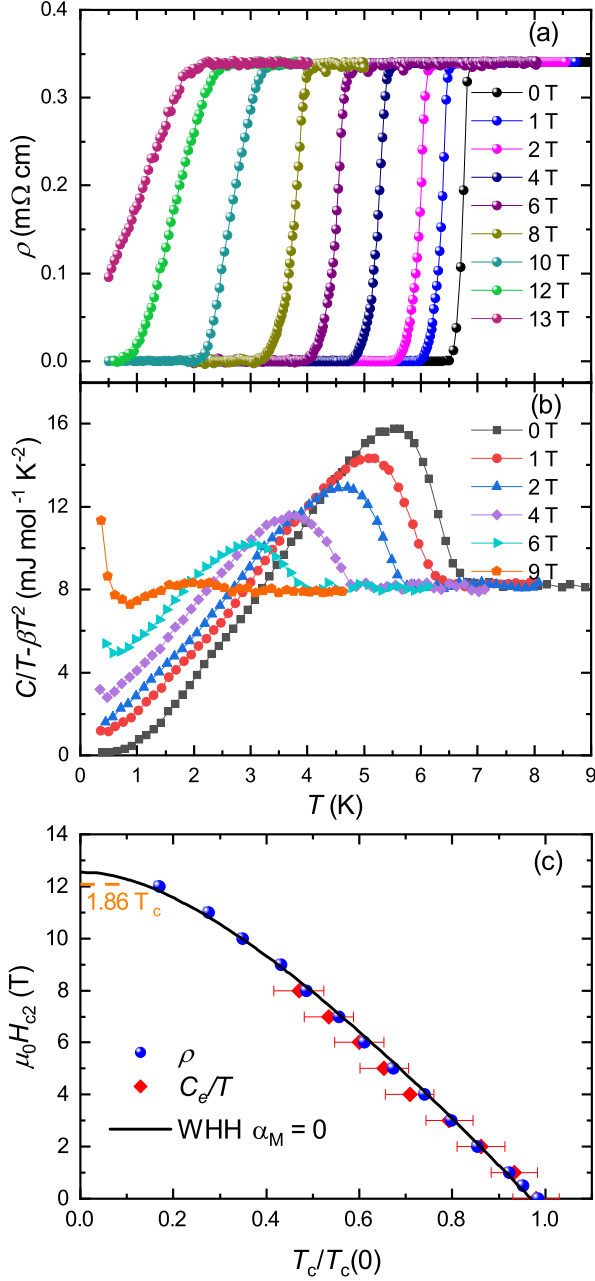


FIG. 5. Temperature dependence of the electrical resistivity (a) and specific heat (b) of NbReSi under various magnetic fields up to 13 T. To better show the superconducting transitions, the phonon contribution  $\beta T^2$  was subtracted from the specific heat. (c) The upper critical field  $H_{c2}$  versus the reduced temperature  $T_c/T_c(0)$  for NbReSi. The solid line represents a fit to the WHH model, while the dashed line marks the Pauli limit.

estimated by  $N(E_F) = 3\gamma_n/\pi^2 k_B^2$  [48], which yields  $N(E_F) = 3.47 \text{ states eV}^{-1} \text{ f.u.}^{-1}$ .

After subtracting the phonon contribution, the zero-field electronic specific heat  $C_e/T$  of NbReSi is shown in Fig. 4 as a function of temperature. The scaled specific jump at  $T_c$ ,  $\Delta C/\gamma_n T_c = 1.18$ , is smaller than the BCS

value of 1.43. The reduced specific-heat jump at  $T_c$  is typically attributed to multiband SC or gap anisotropy. The contribution of SC to the electronic specific heat can be calculated via  $C_e/T = dS/dT$ , where  $S$  is the entropy and can be written as [49]:

$$S(T) = -\frac{3\gamma_n}{k_B \pi^3} \int_0^{2\pi} \int_0^\infty [(1-f)\ln(1-f) + f\ln f] d\epsilon d\phi. \quad (2)$$

Here  $f = (1 + e^{E/k_B T})^{-1}$  is the Fermi function and  $E = \sqrt{\epsilon^2 + \Delta^2(T)}$ . The temperature-dependent superconducting energy gap is approximated to  $\Delta(T) = \Delta(0) \tanh 1.82[1.018(T_c/T - 1)]^{0.51}$ , where  $\Delta(0)$  is the superconducting gap at 0 K. The red solid line in Fig. 4 represents a fit to the single-gap  $s$ -wave model. The derived gap value  $\Delta(0) = 1.75 k_B T_c$  is close to the BCS value of  $1.76 k_B T_c$ , implying weak-coupling SC. It is noted that single-gap behaviors have been reported in other noncentrosymmetric Re-based superconductors, e.g.,  $\text{Re}_6(\text{Ti}, \text{Zr}, \text{Hf})$  [50–52],  $\text{Re}_{24}\text{Ti}_5$  [32],  $\text{Re}_{0.82}\text{Nb}_{0.18}$  [33, 53],  $\text{Re}_3\text{W}$  [54], and  $\text{TaReSi}$  [55].

To study the upper critical field  $H_{c2}$  of NbReSi, the electrical resistivity and heat capacity were measured under various applied magnetic fields up to 13 T. As shown in Figs. 5(a) and (b), the superconducting transitions are gradually suppressed to lower temperatures and become broader with increases the magnetic field. When the magnetic field is larger than 4 T, the specific heat starts to show an upturn at low temperatures, which becomes more prominent as increasing field and is likely due to the nuclear Schottky anomaly. With such an upturn anomaly, it is difficult to precisely determine the field dependence of the specific heat coefficient that might provide important insights into the gap symmetry. The upper critical field of NbReSi extracted from the electrical resistivity and specific heat are displayed in Fig. 5(c) as a function of the reduced temperature  $T_c/T_c(0)$ . Here  $T_c$  is determined as the temperature where zero resistivity is reached, while for the specific heat, it is defined as the midpoint of specific-heat jump. The  $H_{c2}$  values determined using different techniques are highly consistent. It can be seen that the electrical resistivity reaches zero value before cooling to the lowest temperature in a field of 12 T, while in the 13 T curve the transition can still be observed, indicating that the upper critical field  $H_{c2}(0)$  at zero temperature is slightly larger than the weak coupling Pauli limit value of  $1.86 T_c = 12.1$  T. Moreover, the data agree well with the Werthamer-Helfand-Hohenberg (WHH) model in the absence of paramagnetic limiting (i.e., with a Maki parameter  $\alpha_M = 0$ ) [56], yielding a zero-temperature value of  $\mu_0 H_{c2}(0) = 12.6$  T. The upper critical field larger than the weak-coupling Pauli limit has been reported in some other NCSCs, e.g.,  $(\text{Nb}, \text{Ta})\text{Rh}_2\text{B}_2$  [14] and  $\text{K}_2\text{Cr}_3\text{As}_3$  [15] and  $\text{Y}_2\text{C}_3$  [57]. These results suggest the possibility that the effects of paramagnetic limiting may be reduced or



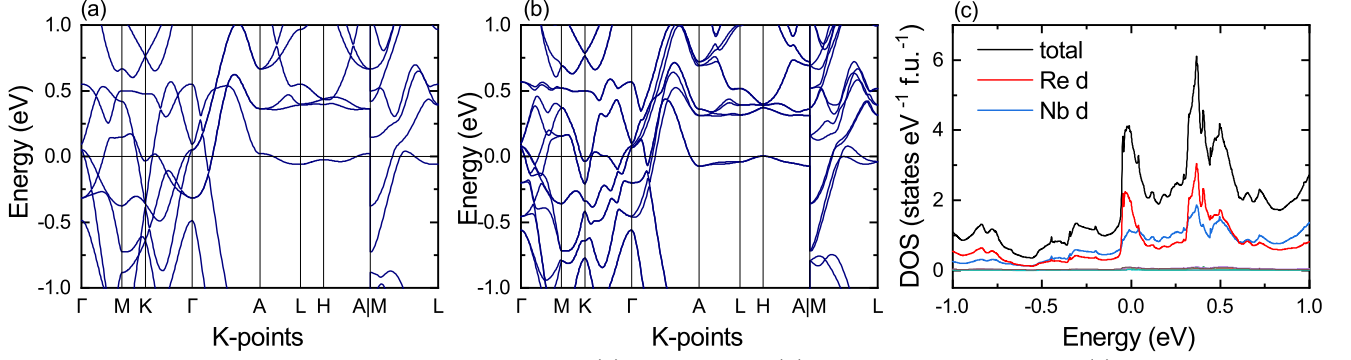


FIG. 6. Electronic band structure of NbReSi, calculated (a) without, and (b) with spin orbit coupling. (c) The total and partial (Re 5d and Nb 4d orbitals) densities of states near the Fermi level when SOC is considered.

absent in NbReSi superconductor. This can arise due to the Cooper pairs having a finite zero-temperature spin-susceptibility, which is a feature of both triplet SC and the admixture of spin-singlet and spin-triplet NCSCs under the influence of strong ASOC [3]. Alternatively, paramagnetic limiting fields larger than  $1.86T_c$  can also arise from a superconducting gap larger than the weak-coupling value, or deviations of the  $g$ -factor from the free electron value  $g = 2$  [2, 58]. While the former appears unlikely from our specific-heat analysis, confirmation of such a finite spin susceptibility requires studying the anisotropy of the upper critical fields, and utilizing nuclear magnetic resonance (NMR) to examine the Knight shift.

The Ginzburg-Landau (GL) coherence length  $\xi_{GL}$  can be calculated from the upper critical field  $\mu_0 H_{c2}(0)$  using

$$\mu_0 H_{c2}(0) = \frac{\Phi_0}{2\pi\xi_{GL}^2}, \quad (3)$$

where  $\Phi_0$  is the magnetic flux quantum, yielding  $\xi_{GL} = 5.11$  nm for NbReSi. The magnetic penetration depth  $\lambda_{GL} = 243.8$  nm can be obtained via:

$$\mu_0 H_{c1}(0) = \frac{\Phi_0}{4\pi\lambda_{GL}^2} \ln \frac{\lambda_{GL}}{\xi_{GL}}. \quad (4)$$

The GL parameter  $\kappa_{GL} = \lambda_{GL}/\xi_{GL} = 49.3$  is much larger than the threshold value of  $1/\sqrt{2}$ , indicating that NbReSi is a strongly type-II superconductor. The thermodynamic critical field  $\mu_0 H_c(0)$  can be estimated from

$$\mu_0 H_{c1}(0)\mu_0 H_{c2}(0) = \mu_0 H_c(0)^2 \ln \kappa_{GL}, \quad (5)$$

yielding a value of 181 mT for NbReSi.

To get more insight into the underlying electronic properties of NbReSi, we also performed the electronic band-structure calculations based on DFT, with and without considering the spin-orbit coupling. As shown in Fig. 6, several bands crossing the Fermi level can be identified. By taking into account the SOC, the band splitting  $E_{ASOC}$  near the Fermi level is estimated to be 180 meV. Its energy scale to the superconducting energy gap, i.e.,

$E_{ASOC}/k_B T_c \sim 350$ , is relatively large compared with many other NCSC [3]. Such a large band splitting suggests an significant effect of ASOC. Relatively more obvious band splitting along  $c$ -axis related to the high symmetry lines  $\Gamma$ -A and M-L suggest a possible anisotropy in NbReSi, which remains verified on single crystal measurements. Figure 6(c) shows the total and partial density of states (DOS) for NbReSi within the energy scale of -1 to 1 eV. The calculated DOS at the Fermi level  $N(E_F) \sim 3.94$  states eV<sup>-1</sup> f.u.<sup>-1</sup> is compatible with the value 3.47 states eV<sup>-1</sup> f.u.<sup>-1</sup> determined from the normal-state electronic specific-heat coefficient. The contributions to  $N(E_F)$  mainly arise from Re-5d and Nb-4d orbits, while the contributions from other orbits or orbits of Si atoms are negligible. Both Re 5d and Nb 4d orbits exhibit relatively large SOC, which results in the large band splitting near the Fermi level.

In noncentrosymmetric superconductors, the ASOC in principle can lift the degeneracy of the electronic bands and thus, the admixture of spin-singlet and spin-triplet pairing states is allowed. For NbReSi, the specific-heat results suggest a fully-gapped superconducting state, more consistent with spin-singlet pairing. To further understand the superconducting pairings and the effect of ASOC in NbReSi, the  $\mu$ SR or NMR studies will be very helpful. For comparison, the superconducting- and normal-state properties of NbReSi, as well as the recently reported NCSC TaReSi are summarized in Table I. Different from NbReSi, TaReSi crystallizes in an orthorhombic TiFeSi-type structure (*Ima2*, No. 46) (see Table. I) [55]. Though TaReSi exhibits a comparable  $T_c$  value to NbReSi and fully-gapped SC, its upper critical field is much smaller, well below the Pauli limit, i.e.,  $H_{c2}/H_p \sim 0.68$ . Whether such distinct upper critical fields in these two compounds are related to the strength of ASOC or other factors requires further investigations.

The large  $H_{c2}$  that is comparable to the Pauli limit seems to be a general feature in Re-based superconducting alloys, including the  $\alpha$ -Mn type materials and NbReSi, and centrosymmetric Re<sub>3</sub>W, in spite of the preserved or broken TRS in their superconducting states [3,

TABLE I. Superconducting and normal-state properties of NbReSi and TaReSi. Data of TaReSi were taken from Ref. 55

Parameters	Unit	NbReSi	TaReSi
Space group	-	$P\bar{6}2m$	$Ima2$
$T_c$	K	6.5	5.32
$\mu_0 H_{c1}(0)$	mT	10.1	6.27
$\mu_0 H_{c2}(0)$	T	12.6	6.6
$\mu_0 H_c(0)$	mT	181	114
$\mu_0 H_P(0)$	T	12.1	9.73
$\lambda_{GL}(0)$	Å	2519	3373
$\xi_{GL}(0)$	Å	51	137
$\theta_D$	K	331	338
$N(E_F)$	states eV <sup>-1</sup> f.u. <sup>-1</sup>	3.94	2.28
$\Delta C_{el}/\gamma_n T_c$	-	1.18	1.07
$\Delta(0)/k_B T_c$	-	1.75	1.4

59, 60]. The origin of a large  $H_{c2}$  is not yet fully understood. It is also possible that the  $H_{c2}$  can be enhanced due to the presence of disorder and nonmagnetic impurities [61]. The upper critical field exceeds the weak coupling Pauli limit in NbReSi, but the determination of whether paramagnetic limiting is weakened or absent in this compound requires further studies on high-quality single crystal.

In addition, the observation of TRS breaking in some Re-based superconductors suggests an important role played by Re. While the previous  $\mu$ SR studies on the Re-free ZrNiAl-type ZrRuAs and LaPdIn suggest a preserved TRS in their superconducting states [41, 42]. Therefore, it is of particular interest to determine whether the TRS is broken in the superconducting state of NbReSi, which might further shed light on the origin of TRS breaking in the Re-based superconductor.

## SUMMARY

To summarize, the noncentrosymmetric NbReSi superconductor were synthesized and investigated by means of the electrical-resistivity, magnetization, and heat-capacity measurements, as well as via electronic band structure calculations. We found that NbReSi shows bulk superconductivity at  $T_c = 6.5$  K. Its upper critical field  $\mu_0 H_{c2}(0) = 12.6$  T is comparable to the weak coupling Pauli limit. The low-temperature zero-field electronic specific heat data suggest nodeless SC, with a gap value close to the BCS theoretical value. The specific-heat discontinuity and the electron-phonon coupling constant  $\lambda_{ep}$  suggest weak-coupling SC in NbReSi. Electronic band structure calculations reveal a relatively large band splitting near the Fermi level due to the presence of a strong ASOC. These results suggest that NbReSi represents a new candidate material to study the broken TRS in the superconducting state of weakly correlated NCSCs.

## ACKNOWLEDGMENTS

This work was supported by the Key R&D Program of Zhejiang Province, China (2021C01002), the National Natural Science Foundation of China (No. 11874320, No. 12034017, and No. 11974306), and the National Key R&D Program of China (No. 2017YFA0303100). T. Shang acknowledge the support from the Natural Science Foundation of Shanghai (Grant No. 21ZR1420500 and No. 21JC1402300).

\* Corresponding author: [tshang@phy.ecnu.edu.cn](mailto:tshang@phy.ecnu.edu.cn)

† Corresponding author: [hqyuan@zju.edu.cn](mailto:hqyuan@zju.edu.cn)

- [1] E. Bauer, G. Hilscher, H. Michor, C. Paul, E. W. Scheidt, A. Griбанov, Y. Seropegin, H. Noël, M. Sigrist, and P. Rogl, Heavy fermion superconductivity and magnetic order in noncentrosymmetric CePt<sub>3</sub>Si, *Phys. Rev. Lett.* **92**, 027003 (2004).
- [2] E. Bauer and M. Sigrist, *Non-centrosymmetric superconductors: introduction and overview*, Vol. 847 (Springer Science & Business Media, 2012).
- [3] M. Smidman, M. B. Salamon, H. Q. Yuan, and D. F. Agterberg, Superconductivity and spin-orbit coupling in non-centrosymmetric materials: a review, *Rep. Prog. Phys.* **80**, 036501 (2017).
- [4] H. Q. Yuan, D. F. Agterberg, N. Hayashi, P. Badica, D. Vandervelde, K. Togano, M. Sigrist, and M. B. Salamon, *s*-wave spin-triplet order in superconductors without inversion symmetry: Li<sub>2</sub>Pd<sub>3</sub>B and Li<sub>2</sub>Pt<sub>3</sub>B, *Phys. Rev. Lett.* **97**, 017006 (2006).
- [5] I. Bonalde, W. Brämer-Escamilla, and E. Bauer, Evidence for line nodes in the superconducting energy gap of noncentrosymmetric CePt<sub>3</sub>Si from magnetic penetration depth measurements, *Phys. Rev. Lett.* **94**, 207002 (2005).
- [6] W. Xie, P. Zhang, B. Shen, W. Jiang, G. Pang, T. Shang, C. Cao, M. Smidman, and H. Yuan, CaPtAs: A new non-centrosymmetric superconductor, *Sci. China Phys. Mech. Astron.* **63**, 237412 (2020).
- [7] T. Shang, M. Smidman, A. Wang, L.-J. Chang, C. Baines, M. K. Lee, Z. Y. Nie, G. M. Pang, W. Xie, W. B. Jiang, M. Shi, M. Medarde, T. Shiroka, and H. Q. Yuan, Simultaneous nodal superconductivity and time-reversal symmetry breaking in the noncentrosymmetric superconductor CaPtAs, *Phys. Rev. Lett.* **124**, 207001 (2020).
- [8] G. M. Pang, M. Smidman, W. B. Jiang, J. K. Bao, Z. F. Weng, Y. F. Wang, L. Jiao, J. L. Zhang, G. H. Cao, and H. Q. Yuan, Evidence for nodal superconductivity in quasi-one-dimensional K<sub>2</sub>Cr<sub>3</sub>As<sub>3</sub>, *Phys. Rev. B* **91**, 220502(R) (2015).
- [9] J. Chen, L. Jiao, J. L. Zhang, Y. Chen, L. Yang, M. Nicklas, F. Steglich, and H. Q. Yuan, Evidence for two-gap superconductivity in the non-centrosymmetric compound LaNiC<sub>2</sub>, *New J. Phys.* **15**, 053005 (2013).
- [10] S. Kuroiwa, Y. Saura, J. Akimitsu, M. Hiraishi, M. Miyazaki, K. H. Satoh, S. Takeshita, and R. Kadono, Multigap superconductivity in sesquicarbides La<sub>2</sub>C<sub>3</sub> and Y<sub>2</sub>C<sub>3</sub>, *Phys. Rev. Lett.* **100**, 097002 (2008).

- [11] A. Harada, S. Akutagawa, Y. Miyamichi, H. Mukuda, Y. Kitaoka, and J. Akimitsu, Multigap superconductivity in  $\text{Y}_2\text{C}_3$ : a  $^{13}\text{C}$ -NMR study, *J. Phys. Soc. Jpn.* **76**, 023704 (2007).
- [12] J. Chen, M. B. Salamon, S. Akutagawa, J. Akimitsu, J. Singleton, J. L. Zhang, L. Jiao, and H. Q. Yuan, Evidence of nodal gap structure in the noncentrosymmetric superconductor  $\text{Y}_2\text{C}_3$ , *Phys. Rev. B* **83**, 144529 (2011).
- [13] N. Kimura, K. Ito, H. Aoki, S. Uji, and T. Terashima, Extremely high upper critical magnetic field of the noncentrosymmetric heavy fermion superconductor  $\text{CeRhSi}_3$ , *Phys. Rev. Lett.* **98**, 197001 (2007).
- [14] E. M. Carnicom, W. Xie, T. Klimczuk, J. Lin, K. Górnicka, Z. Sobczak, N. P. Ong, and R. J. Cava,  $\text{TaRh}_2\text{B}_2$  and  $\text{NbRh}_2\text{B}_2$ : superconductors with a chiral noncentrosymmetric crystal structure, *Sci. Adv.* **4**, eaar7969 (2018).
- [15] T. Kong, S. L. Bud'ko, and P. C. Canfield, Anisotropic  $H_{c2}$ , thermodynamic and transport measurements, and pressure dependence of  $T_c$  in  $\text{K}_2\text{Cr}_3\text{As}_3$  single crystals, *Phys. Rev. B* **91**, 020507(R) (2015).
- [16] Arushi, D. Singh, P. K. Biswas, A. D. Hillier, and R. P. Singh, Unconventional superconducting properties of noncentrosymmetric  $\text{Re}_{5.5}\text{Ta}$ , *Phys. Rev. B* **101**, 144508 (2020).
- [17] N. Kimura, K. Ito, K. Saitoh, Y. Umeda, H. Aoki, and T. Terashima, Pressure-induced superconductivity in noncentrosymmetric heavy-fermion  $\text{CeRhSi}_3$ , *Phys. Rev. Lett.* **95**, 247004 (2005).
- [18] I. Sugitani, Y. Okuda, H. Shishido, T. Yamada, A. Thamizhavel, E. Yamamoto, T. D. Matsuda, Y. Haga, T. Takeuchi, R. Settai, and Y. Onuki, Pressure-induced heavy-fermion superconductivity in antiferromagnet  $\text{CeIrSi}_3$  without inversion symmetry, *J. Phys. Soc. Jpn.* **75**, 043703 (2006).
- [19] R. Settai, I. Sugitani, Y. Okuda, A. Thamizhavel, M. Nakashima, Y. Onuki, and H. Harima, Pressure-induced superconductivity in  $\text{CeCoGe}_3$  without inversion symmetry, *J. Magn. Magn. Mater.* **310**, 844 (2007).
- [20] F. Honda, I. Bonalde, S. Yoshiuchi, Y. Hirose, T. Nakamura, K. Shimizu, R. Settai, and Y. Onuki, Pressure-induced superconductivity in non-centrosymmetric compound  $\text{CeIrGe}_3$ , *Physica C* **470**, S543 (2010).
- [21] T. Akazawa, H. Hidaka, T. Fujiwara, T. C. Kobayashi, E. Yamamoto, Y. Haga, R. Settai, and Y. Onuki, Pressure-induced superconductivity in ferromagnetic  $\text{UIr}$  without inversion symmetry, *J. Phys.: Condens. Matter* **16**, L29 (2004).
- [22] H. Takeya, M. ElMassalami, S. Kasahara, and K. Hirata, Specific-heat studies of the spin-orbit interaction in noncentrosymmetric  $\text{Li}_2(\text{Pd}_{1-x}\text{Pt}_x)_3\text{B}$  ( $x = 0, 0.5, 1$ ) superconductors, *Phys. Rev. B* **76**, 104506 (2007).
- [23] M. Nishiyama, Y. Inada, and G.-q. Zheng, Spin triplet superconducting state due to broken inversion symmetry in  $\text{Li}_2\text{Pt}_3\text{B}$ , *Phys. Rev. Lett.* **98**, 047002 (2007).
- [24] A. D. Hillier, J. Quintanilla, and R. Cywinski, Evidence for time-reversal symmetry breaking in the noncentrosymmetric superconductor  $\text{LaNiC}_2$ , *Phys. Rev. Lett.* **102**, 117007 (2009).
- [25] T. Shang, S. K. Ghosh, J. Z. Zhao, L.-J. Chang, C. Baines, M. K. Lee, D. J. Gawryluk, M. Shi, M. Medarde, J. Quintanilla, and T. Shiroka, Time-reversal symmetry breaking in the noncentrosymmetric  $\text{Zr}_3\text{Ir}$  superconductor, *Phys. Rev. B* **102**, 020503(R) (2020).
- [26] Arushi, D. Singh, A. D. Hillier, M. S. Scheurer, and R. P. Singh, Time-reversal symmetry breaking and multigap superconductivity in the noncentrosymmetric superconductor  $\text{La}_7\text{Ni}_3$ , *Phys. Rev. B* **103**, 174502 (2021).
- [27] D. Singh, M. S. Scheurer, A. D. Hillier, D. T. Adroja, and R. P. Singh, Time-reversal-symmetry breaking and unconventional pairing in the noncentrosymmetric superconductor  $\text{La}_7\text{Rh}_3$ , *Phys. Rev. B* **102**, 134511 (2020).
- [28] D. A. Mayoh, A. D. Hillier, G. Balakrishnan, and M. R. Lees, Evidence for the coexistence of time-reversal symmetry breaking and bardeen-cooper-schrieffer-like superconductivity in  $\text{La}_7\text{Pd}_3$ , *Phys. Rev. B* **103**, 024507 (2021).
- [29] J. A. T. Barker, D. Singh, A. Thamizhavel, A. D. Hillier, M. R. Lees, G. Balakrishnan, D. M. Paul, and R. P. Singh, Unconventional superconductivity in  $\text{La}_7\text{Ir}_3$  revealed by muon spin relaxation: Introducing a new family of noncentrosymmetric superconductor that breaks time-reversal symmetry, *Phys. Rev. Lett.* **115**, 267001 (2015).
- [30] R. P. Singh, A. D. Hillier, B. Mazidian, J. Quintanilla, J. F. Annett, D. M. Paul, G. Balakrishnan, and M. R. Lees, Detection of time-reversal symmetry breaking in the noncentrosymmetric superconductor  $\text{Re}_6\text{Zr}$  using muon-spin spectroscopy, *Phys. Rev. Lett.* **112**, 107002 (2014).
- [31] D. Singh, J. A. T. Barker, A. Thamizhavel, D. M. Paul, A. D. Hillier, and R. P. Singh, Time-reversal symmetry breaking in the noncentrosymmetric superconductor  $\text{Re}_6\text{Hf}$ : further evidence for unconventional behavior in the  $\alpha$ -Mn family of materials, *Phys. Rev. B* **96**, 180501(R) (2017).
- [32] T. Shang, G. M. Pang, C. Baines, W. B. Jiang, W. Xie, A. Wang, M. Medarde, E. Pomjakushina, M. Shi, J. Mesot, H. Q. Yuan, and T. Shiroka, Nodeless superconductivity and time-reversal symmetry breaking in the noncentrosymmetric superconductor  $\text{Re}_{24}\text{Ti}_5$ , *Phys. Rev. B* **97**, 020502(R) (2018).
- [33] T. Shang, M. Smidman, S. K. Ghosh, C. Baines, L. J. Chang, D. J. Gawryluk, J. A. T. Barker, R. P. Singh, D. M. Paul, G. Balakrishnan, E. Pomjakushina, M. Shi, M. Medarde, A. D. Hillier, H. Q. Yuan, J. Quintanilla, J. Mesot, and T. Shiroka, Time-reversal symmetry breaking in Re-based superconductors, *Phys. Rev. Lett.* **121**, 257002 (2018).
- [34] A. A. Aczel, T. J. Williams, T. Goko, J. P. Carlo, W. Yu, Y. J. Uemura, T. Klimczuk, J. D. Thompson, R. J. Cava, and G. M. Luke, Muon spin rotation/relaxation measurements of the noncentrosymmetric superconductor  $\text{Mg}_{10}\text{Ir}_{19}\text{B}_{16}$ , *Phys. Rev. B* **82**, 024520 (2010).
- [35] D. Singh, J. A. T. Barker, A. Thamizhavel, A. D. Hillier, D. M. Paul, and R. P. Singh, Superconducting properties and  $\mu\text{SR}$  study of the noncentrosymmetric superconductor  $\text{Nb}_{0.5}\text{Os}_{0.5}$ , *J. Phys.: Condens. Mat.* **30**, 075601 (2018).
- [36] T. Shang, C. Baines, L.-J. Chang, D. J. Gawryluk, E. Pomjakushina, M. Shi, M. Medarde, and T. Shiroka,  $\text{Re}_{1-x}\text{Mo}_x$  as an ideal test case of time-reversal symmetry breaking in unconventional superconductors, *npj Quantum Mater.* **5**, 76 (2020).
- [37] T. Shang, W. Xie, J. Z. Zhao, Y. Chen, D. J. Gawryluk, M. Medarde, M. Shi, H. Q. Yuan, E. Pomjakushina, and T. Shiroka, Multigap superconductivity in centrosymmetric and noncentrosymmetric rhenium-boron superconductors, *Phys. Rev. B* **103**, 184517 (2021).

- [38] H. Barz, H. C. Ku, G. P. Meisner, Z. Fisk, and B. T. Matthias, Ternary transition metal phosphides: High-temperature superconductors, *Proc. Natl. Acad. Sci. U.S.A.* **77**, 3132 (1980).
- [39] G. Meisner, H. Ku, and H. Barz, Superconducting equiatomic ternary transition metal arsenides, *Mater. Res. Bull.* **18**, 983 (1983).
- [40] I. Shirotni, K. Tachi, Y. Konno, S. Todo, and T. Yagi, Superconductivity of the ternary ruthenium compounds HfRuP and ZrRuX (X = P, As, Si or Ge) prepared at a high pressure, *Philos. Mag. B* **79**, 767 (1999).
- [41] D. Das, D. T. Adroja, M. R. Lees, R. W. Taylor, Z. S. Bishnoi, V. K. Anand, A. Bhattacharyya, Z. Guguchia, C. Baines, H. Luetkens, G. B. G. Stenning, L. Duan, X. Wang, and C. Jin, Probing the superconducting gap structure in the noncentrosymmetric topological superconductor ZrRuAs, *Phys. Rev. B* **103**, 144516 (2021).
- [42] H. Su, Z. Y. Nie, F. Du, S. S. Luo, A. Wang, Y. J. Zhang, Y. Chen, P. K. Biswas, D. T. Adroja, C. Cao, M. Smidman, and H. Q. Yuan, Fully gapped superconductivity with preserved time-reversal symmetry in noncentrosymmetric LaPdIn, *Phys. Rev. B* **104**, 024505 (2021).
- [43] Y. P. Yarmolyuk and E. I. Gladishevs'kii, New ternary compounds of equiatomic composition in the systems of two transition metals and silicon or germanium, *Dopov. Akad. Nauk Ukr. RSR, Ser. B*, **11**, 1030 (1974).
- [44] A. Aharoni, Demagnetizing factors for rectangular ferromagnetic prisms, *J. Appl. Phys.* **83**, 3432 (1998).
- [45] J. A. Osborn, Demagnetizing Factors of the General Ellipsoid, *Phys. Rev.* **67**, 351 (1945).
- [46] G. V. S. Rao, K. Wagner, G. Balakrishnan, J. Janaki, W. Paulus, R. Schöllhorn, V. S. Subramanian, and U. Poppe, Structure and superconductivity studies on ternary equiatomic silicides, *MM'Si*, *Bull. Mater. Sci.* **7**, 215 (1985).
- [47] W. L. McMillan, Transition temperature of strong-coupled superconductors, *Phys. Rev.* **167**, 331 (1968).
- [48] C. Kittel, P. McEuen, and P. McEuen, *Introduction to solid state physics*, Vol. 8 (Wiley New York, 1996).
- [49] M. Tinkham, *Introduction to superconductivity* (Courier Corporation, 2004).
- [50] D. Singh, K. P. Sajilesh, J. A. T. Barker, D. M. Paul, A. D. Hillier, and R. P. Singh, Time-reversal symmetry breaking in the noncentrosymmetric superconductor Re<sub>6</sub>Ti, *Phys. Rev. B* **97**, 100505(R) (2018).
- [51] D. A. Mayoh, J. A. T. Barker, R. P. Singh, G. Balakrishnan, D. M. Paul, and M. R. Lees, Superconducting and normal-state properties of the noncentrosymmetric superconductor Re<sub>6</sub>Zr, *Phys. Rev. B* **96**, 064521 (2017).
- [52] D. Singh, A. D. Hillier, A. Thamizhavel, and R. P. Singh, Superconducting properties of the noncentrosymmetric superconductor Re<sub>6</sub>Hf, *Phys. Rev. B* **94**, 054515 (2016).
- [53] J. Chen, L. Jiao, J. L. Zhang, Y. Chen, L. Yang, M. Nicklas, F. Steglich, and H. Q. Yuan, BCS-like superconductivity in the noncentrosymmetric compounds Nb<sub>x</sub>Re<sub>1-x</sub> (0.13 ≤ x ≤ 0.38), *Phys. Rev. B* **88**, 144510 (2013).
- [54] P. K. Biswas, A. D. Hillier, M. R. Lees, and D. M. Paul, Comparative study of the centrosymmetric and noncentrosymmetric superconducting phases of Re<sub>3</sub>W using muon spin spectroscopy and heat capacity measurements, *Phys. Rev. B* **85**, 134505 (2012).
- [55] K. P. Sajilesh and R. P. Singh, Superconducting properties of the non-centrosymmetric superconductors TaXSi (X = Re, Ru), *Supercond. Sci. Technol.* **34**, 055003 (2021).
- [56] N. R. Werthamer, E. Helfand, and P. C. Hohenberg, Temperature and purity dependence of the superconducting critical field, *H<sub>c2</sub>*. iii. electron spin and spin-orbit effects, *Phys. Rev.* **147**, 295 (1966).
- [57] H. Yuan, J. Chen, J. Singleton, S. Akutagawa, and J. Akimitsu, Large upper critical field in noncentrosymmetric superconductor Y<sub>2</sub>C<sub>3</sub>, *J. Phys. Chem. Solids* **72**, 577 (2011).
- [58] A. M. Clogston, Upper limit for the critical field in hard superconductors, *Phys. Rev. Lett.* **9**, 266 (1962).
- [59] P. K. Biswas, M. R. Lees, A. D. Hillier, R. I. Smith, W. G. Marshall, and D. M. Paul, Structure and superconductivity of two different phases of Re<sub>3</sub>W, *Phys. Rev. B* **84**, 184529 (2011).
- [60] T. Shang and T. Shiroka, Time-reversal symmetry breaking in Re-based superconductors: recent developments, *Front. Phys.* **9**, 270 (2021).
- [61] A. Gurevich, Enhancement of the upper critical field by nonmagnetic impurities in dirty two-gap superconductors, *Phys. Rev. B* **67**, 184515 (2003).